metals

Article

Effects of Quenching and Tempering Heat Treatment Processing on the Microstructure and Properties of High-Strength Hull Steel

Hongmei Zhang [1,†], Mingshuai Huo [2,*,†], Zhiqiang Ma [1], Hui Wu [2], Guanqiao Su [2], Lianjie Li [2], Tao Zhang [2], Fei Lin [2], Fenghua Chen [2] and Zhengyi Jiang [1,2,*]

1 School of Material and Metallurgy, University of Science and Technology Liaoning, Anshan 114051, China; zhanghm@ustl.edu.cn (H.Z.); mazhiq2022@hotmail.com (Z.M.)
2 School of Mechanical, Materials, Mechatronic and Biomedical Engineering, University of Wollongong, Wollongong, NSW 2522, Australia; hwu@uow.edu.au (H.W.); suhangjoe@gmail.com (G.S.); ll940@uowmail.edu.au (L.L.); tz570@uowmail.edu.au (T.Z.); fl236@uowmail.edu.au (F.L.); fc998@uowmail.edu.au (F.C.)
* Correspondence: mhuo@uow.edu.au (M.H.); jiang@uow.edu.au (Z.J.)
† These authors contributed equally to this work.

Abstract: The construction of heavy polar icebreakers is usually done with special hull steels, which require comprehensive properties such as good low-temperature toughness, high strength, and superior fatigue resistance. Reasonable and satisfactory heat treatments should be investigated and applied to acquire the required high strength and superior low-temperature toughness, since this is deemed an effective approach to ameliorate the combined properties of high-strength hull steels. Regarding this, the present study specifically explores the effects of different laboratory-based quenching (850 to 930 °C) and tempering (580 to 660 °C) heat treatments on the final low-temperature toughness of the high-strength hull steels. The low-temperature toughness is eventually improved without significantly sacrificing the strength. The results show that a favourable combination of properties can be obtained in the specimens under 900 °C quenching and 660 °C tempering processes. Additionality, the specimens tempered at 620 °C present the highest hardness, owing to the higher percentage of tempered martensite. Detailed mechanisms of the enhanced properties of the typical specimens subjected to the corresponding quenching and tempering processing are analysed and explicated.

Keywords: high-strength hull steel; quenching and tempering heat treatment processing; microstructure evolution; low-temperature toughness

Citation: Zhang, H.; Huo, M.; Ma, Z.; Wu, H.; Su, G.; Li, L.; Zhang, T.; Lin, F.; Chen, F.; Jiang, Z. Effects of Quenching and Tempering Heat Treatment Processing on the Microstructure and Properties of High-Strength Hull Steel. *Metals* **2022**, *12*, 914. https://doi.org/10.3390/met12060914

Academic Editors: David Rojas and Andrea Di Schino

Received: 21 March 2022
Accepted: 24 May 2022
Published: 26 May 2022

1. Introduction

With the rapid expansion of human economic activities, fast growth of the population, and exhaustion of land resources, the survival and development of human beings will depend more and more on the oceans' resources. Human activities in these waters inevitably face sea ice problems. Sea ice mainly exists in the middle and high latitudes. The harm to human economic activities at sea can be divided into two categories: collision between ships sailing in the sea, and ice and icebergs floating on the ocean surface. During the freezing period, the ice freezes in the sea, blocking ports, waterways, and large areas of the sea, causing all kinds of ships and marine engineering buildings to be trapped, and their structures to suffer compression damage. Collision between the hull body and the ice is quite serious. At the moment of collision, the hull structure is subjected to a huge impact load, which may cause severe damage. As a result, this can cause structural safety problems such as water intake in ship cabins, damage to ship cabins, hull breakage, or sinking, environmental concerns such as oil and gas leakage, and safety hazards for crew members [1,2].

Polar icebreakers—especially heavy icebreakers—cannot be built without key materials, and are usually made of special steels such as low-temperature hull steel that can adapt to the harsh polar service environment (mostly between −60 and −40 °C) [3]. The hull below the contact line with ice is usually made of special steels with the highest requirements. This part of the hull must be able to withstand repeated impacts with ice, and must have sufficient low-temperature toughness, strength, weldability, fatigue strength, and other comprehensive properties. In this regard, an increasing number of industrial shipping applications—especially in the polar regions—have driven the continuing demand for special hull steels that can offer both high strength and low-temperature toughness to ensure the safety of icebreakers. As a consequence, a growing number of researchers, engineers, and manufacturers are striving to produce different grades of hull steels and optimise their production lines [4–7]. Among them, EH47 is a typical hull steel that holds an extraordinary combination of mechanical properties for diverse applications in the transport, construction, and shipbuilding industries, as well as offshore platform facilities [8].

Various heat treatment strategies greatly influence the microstructural morphology, resulting in different final properties of steels [9]. Among them, precise control of temperature and duration for the quenching and tempering processes is imperative to achieve the desired balance of constitutive microstructural and mechanical properties. For most low-alloy steels, ferrite and pearlite can be acquired via slow cooling. Generally, the pearlite always encompasses the lamellar clusters of ferrite and cementite. With a higher cooling rate, an upper bainite microstructure can be attained from austenite. The upper bainite normally includes ferrite platelets hindered by austenite or carbides. Meanwhile, these types of microstructures can be observed and characterised through their particular "C-curve" based on the well-known time–temperature transformation (TTT) diagrams. It has been documented that carbides may precipitate from the carbon-supersaturated austenite, while they can also precipitate from enriched ferrite plates in the lower bainite [10]. In contrast, martensite will be obtained when a further increase in the cooling rate is applied, which usually involves a number of carbon-supersaturated ferrite platelets with a high density of dislocations or twin boundaries [11,12]. It should be noted that the residual austenite always exists along the martensite lath boundaries, and can be more homogeneous and detached compared to the original structure. After tempering, the residual austenite disintegrates and maintains the state of fine and even distribution.

In general, low tempering temperatures may simply lessen the internal stresses, diminishing brittleness while mostly preserving the hardness levels [13]. Nevertheless, in some low-alloy steels containing certain elements, such as Cr and Mo, hardness may increase even when tempered at low temperatures. Many steels with high contents of such alloying elements act similarly to precipitation-hardening alloys, which show the opposite effects observed in quenching and tempering processes. In comparison, tempering at higher temperatures tends to cause a greater reduction in hardness, but leads to increased elasticity and plasticity by sacrificing a certain amount of strength. However, the steel may suffer from another embrittlement phase, known as "temper embrittlement", which arises once the steel is kept for too long within the temperature interval of temper embrittlement. When heated above this temperature, the steel will usually be quickly cooled down to avoid the occurrence of temper embrittlement.

Evidently, it is incredibly important to clarify the potential mechanisms in different heat treatment strategies that may have a close relationship with the key low-temperature properties and service life. Precise controls of temperature and duration for the quenching and tempering are imperative to achieve the desired balance of constitutive microstructural and mechanical properties. To date, although some scholars have carried out research on the heat treatment of some hull steels, the underlying mechanisms are not understood in detail. The present work is concerned with specific elaboration of the strengthening mechanisms of high-strength EH47 hull steel subjected to different kinds of laboratory-based quenching and tempering processes. The following research consists of the results comparison and corresponding analyses of microstructure and microtexture evolution, low-temperature toughness and hardness alterations, fractographic features, and crystallographic investigation.

2. Materials and Methods

High-strength EH47 hull steel with a surface roughness (R_a) of 0.04 µm was the as-received material in this study. The chemical composition of the EH47 steel used in the current research work, by weight percentage, is listed in Table 1. Heat treatment processing is essential, and plays a key role in achieving the excellent combination of strength and toughness of the high-strength hull steel. In this case, various laboratory-based heat treatment strategies comprising different quenching and tempering processes were carried out. To develop a reasonable heat treatment process, the critical temperatures of A_{c1} and A_{c3} were initially determined by the empirical formulae given in [12] Equations (1) and (2), considering the effects of different alloying elements in EH47 steel. The calculated A_{c1} and A_{c3} values were 723 and 905 °C, respectively. Then, detailed strategies and parameters for all of the heat treatment processes were proposed, as shown in Figure 1 and Table 2. Normally, the quenching temperature is above A_{c3} to meet the requirements of steel production [14]. However, in the present study, the quenching temperatures were selected from 850 to 930 °C to comprehensively clarify the influences of different microstructural constituents, and the tempering temperatures were set to 580, 620, and 660 °C for better understanding of their influence on the final properties of the hull steel. Heat treatment was carried out using a GR.TF60/18 electric vacuum furnace (Guier Machinery Equipment Co., Ltd., Shanghai, China) under an argon atmosphere with a heating rate of 20 °C/min. Each heat treatment process was performed with a soaking time of 30 min once the pre-set quenching/tempering temperature (as shown in Figure 1 and Table 2) was reached. In order to eliminate the oxide scale formed on the specimens' surfaces, the specimens were immediately quenched to room temperature in a water tank after soaking, and then cleaned carefully with ethanol, followed by ultrasonic treatment for 20 min.

$$A_{c1} = 723 - 10.7\mathrm{Mn} - 16.9\mathrm{Ni} + 29.1\mathrm{Si} + 16.9\mathrm{Cr} + 290\mathrm{As} + 6.38\mathrm{W}. \quad (1)$$

$$A_{c3} = 910 - 203\sqrt{\mathrm{C}} - 15.2\mathrm{Ni} + 44.7\mathrm{Si} + 104\mathrm{V} + 31.5\mathrm{Mo} + 13.1\mathrm{W}. \quad (2)$$

Table 1. Chemical composition of EH47 steel (wt%).

C	Si	Mn	Cr	Ni	P	S	N	Als	Mo	Nb	V	Ti
0.07	0.16	1.35	0.21	0.66	0.006	0.001	0.004	0.03	0.16	0.03	0.006	0.013

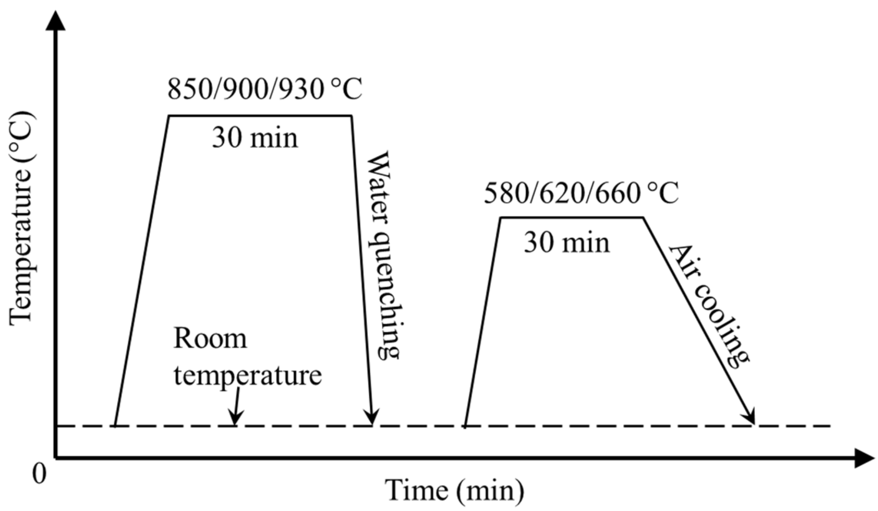

Figure 1. Heat treatment strategies with different quenching and tempering processes.

Table 2. Detailed parameters for various heat treatment processes.

No.	Quenching Temperature (°C)	Soaking Time (min)	Tempering Temperature (°C)	Soaking Time (min)
1	850	30	580	30
2	850	30	620	30
3	850	30	660	30
4	900	30	580	30
5	900	30	620	30
6	900	30	660	30
7	930	30	580	30
8	930	30	620	30
9	930	30	660	30

Vickers hardness was measured by a Q10 M hardness tester (Qness GmbH, Salzburg, Austria) along the specimens' cross-sections (rolling and normal directions) after polishing. Five measurements were taken for each specimen, with a load of 10 kgf and a dwelling time of 10 s. Charpy impact tests were conducted on a JB-300B impact testing machine (Chengyu Testing Equipment Co., Ltd., Jinan, China) with a speed of 5.2 m/s at −40 °C for assessing the low-temperature toughness of the EH47 hull steels after different quenching and tempering heat treatments. The dimensions of each specimen are shown in Figure 2, according to the international standard ISO148-2006. The longitudinal axis of the specimen is parallel to the rolling direction of the steel plate. The length direction of the notch is perpendicular to the rolled surface of the steel plate. Metallographic observations of the cross-sections of specimens in each case were carried out on a VHX-5000 series 3D super-depth digital microscope (Keyence Corporation, Osaka, Japan). The chemical etching in this study was conducted using 4% nital solution with a dwelling time of ~7 s. For characterising the grain structure and crystallographic microtexture, electron-backscattered diffraction (EBSD) tests were performed on a JSM 7001F field-emission scanning electron microscope (FESEM; JEOL, Tokyo, Japan) with 15 kV operating voltage and a 6.5 nA probe current. The FESEM was supplied with an Oxford Instruments Nordlys II (S) camera operating with the AZtec acquisition software suite (FEG-SEM). A step size of 0.1 µm was used such that a region of 50 µm × 40 µm was scanned. Different microstructural data from EBSD tests were processed using Oxford Instruments Channel-5 software. After that, an IGMA HD scanning electron microscope (ZEISS, Jena, Germany) was used for fracture surface observation and EDS analysis. In addition, a JEM 2100 transmission electron microscope (JEOL, Tokyo, Japan) was used for observing more detailed microstructural features of the specimens subjected to different heat treatment strategies.

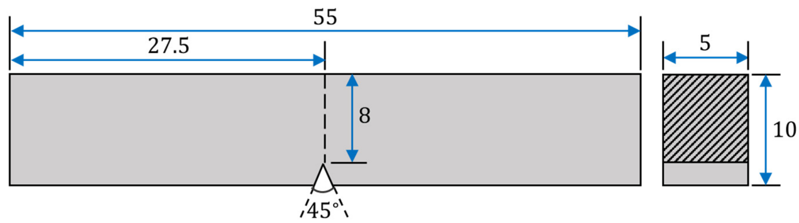

Figure 2. Geometry and dimensions of the low-temperature impact test specimens (unit: mm).

3. Results and Discussion

3.1. Metallography

The microstructure of the as-received high-strength EH47 hull steel is shown in Figure 3. It can be clearly seen that the constituent microstructure mainly comprises polygonal ferrite (white) and pearlite (black). Meanwhile, the grains of both phases present the typical heterogeneous band characterisation hereditary from the rolling process. This is a common phenomenon, since the grains are inevitably elongated along the rolling direction after the hot and cold deformations.

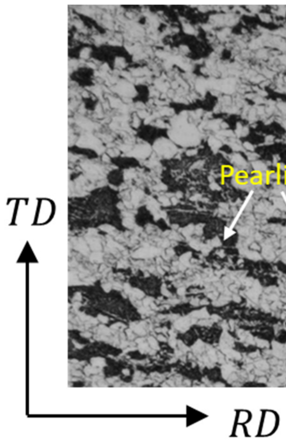

Figure 3. The microstructure of the as-received high-strength EH47 hull steel.

The metallographic microstructure subjected to various quenching and tempering temperatures is shown in Figure 4. In most cases, the microstructure consists of acicular/polygonal ferrite, lath-tempered martensite, and some retained austenite. It can be clearly seen that the microstructure under lower tempering temperatures (Figure 4a,d,g for 580 °C and Figure 4b,e,h for 620 °C) presents higher volume fractions of tempered martensite, which is hereditary from the quenching process. The specimens subjected to the highest tempering temperature (660 °C) have a higher content of ferrite, as shown in Figure 4c,f,i. This is because the recrystallisation phenomenon occurs in the tempered martensite at a relatively high tempering temperature, which unsurprisingly leads to increased ferrite.

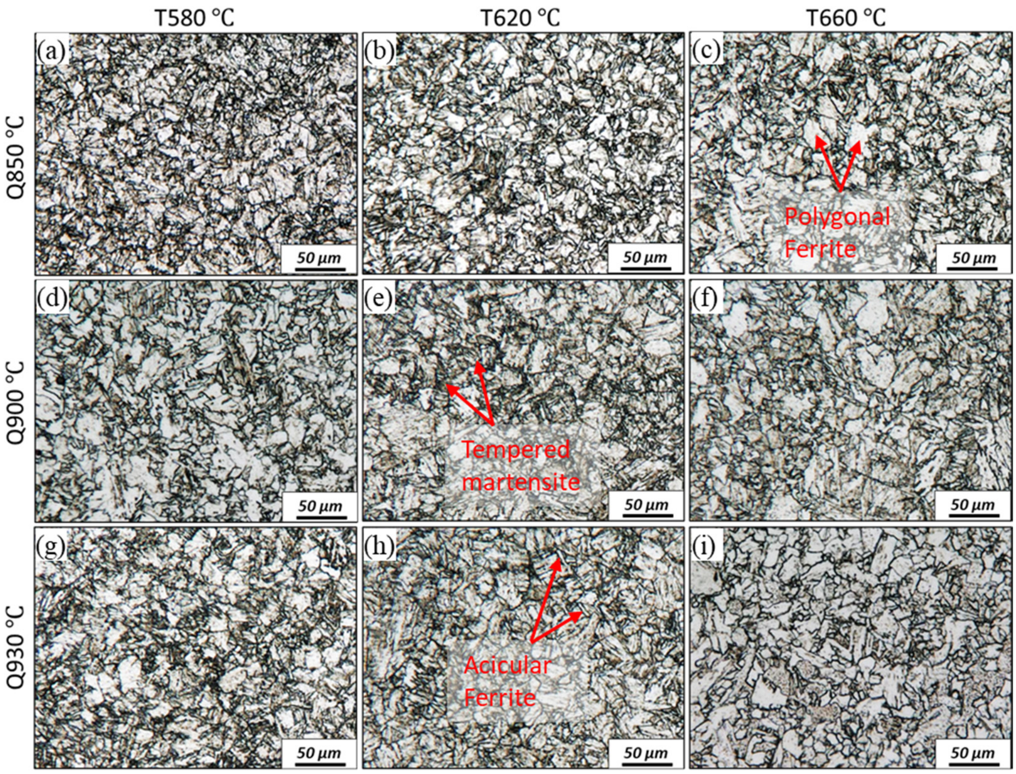

Figure 4. Microstructure of the specimens with different quenching and tempering processes: (**a**) Q850 °C + T580 °C, (**b**) Q850 °C + T620 °C, (**c**) Q850 °C + T660 °C, (**d**) Q900 °C + T580 °C, (**e**) Q900 °C + T620 °C, (**f**) Q900 °C + T660 °C, (**g**) Q930 °C + T580 °C, (**h**) Q930 °C + T620 °C and (**i**) Q930 °C + T660 °C.

Moreover, it can be seen that even higher quenching or tempering temperatures lead to coarsened grain size, and the specimens tempered at lower temperatures (Figure 4a,d,g for 580 °C and Figure 4b,e,h for 620 °C) present obvious heterogeneity of the phase distribution. With the tempering temperature increasing to 620 °C, more carbides are obviously precipitated, as shown in Figure 4c,f,i. The growth of carbides was supposed to occur via Ostwald ripening during the tempering process [10]. In addition, the coarsening process takes place once the minor carbides dissolve into the matrix. Although the microstructure of the tempered martensite appears to be coarsened, the distribution of the microstructure becomes more uniform with the homogeneous distribution of the lath-tempered martensite. The reason for this is that with the increase in quenching temperature, the volume fraction of retained austenite increases. In the process of tempering, the retained austenite gradually breaks down and diffuses at the grain boundary, thus forming the lamellar-tempered martensite. This is a typical γ–α transformation that requires a sufficient amount of carbon. Tempered martensite lath is supposed to be produced from the prior austenite grain boundaries, and the lath is slim and extended, even penetrating the entire grain [15], which always has high-level dislocation density and relatively high hardness. As a result, the mixture of tempered martensite and ferrite can provide a good balance between strength and toughness.

3.2. Mechanical Properties and Fractography

The impact testing results corresponding to different quenching and tempering processes can be found in Figure 5a–c. It is clear that all of the heat treatment processes definitely enhanced the impact properties, regardless of the different quenching and tempering routines being used. With the increase in quenching temperature from 850 to 930 °C, the impact energy presents a decreasing trend, except in the case with 660 °C tempering. One reason for this is that at higher quenching temperatures, more tempered martensites are generated due to the large amount of austenites produced at high intermediate temperatures before quenching. Another reason is due to the coarser grains with the high degree of heterogeneity obtained at high quenching temperatures. The highest impact energy (107.5 J) was found in the case with 900 °C quenching and 660 °C tempering. This should produce the most preferable combination of polygonal ferrite, acicular ferrite, and tempered martensite. Meanwhile, certain tempered sorbites with fine plate perlites may exist in this specimen with the highest tempering temperature being used, which can also contribute to better comprehensive mechanical properties. Moreover, it can be clearly seen that the lowest impact energies are always obtained for the cases tempered at 620 °C. This can be understood from the microstructure results in Figure 4, which shows the highest volume fraction of tempered martensites. This kind of feature has a certain negative influence on the formability of the materials. Since specimen No. 2 (quenched at 850 °C and tempered at 620 °C) and specimen No. 6 (quenched at 900 °C and tempered at 660 °C) obtained the lowest and highest impact energies, respectively, these two specimens were selected to conduct the EBSD tests for subsequent investigation and analysis.

By comparison, specimens treated with the highest quenching temperature (930 °C) always show the lowest impact properties. The main reason for this may be that the grain size of prior austenite increases greatly at high quenching temperatures, significantly coarsening the tempered martensite, and leading to lowered impact properties. Normally, a high tempering temperature leads to the recrystallisation of laminate-tempered martensite, which then transforms to polygonal ferrite. It can be seen that the high-temperature quenching plus relatively low-temperature tempering may significantly refine the grain size. In addition, the tempered martensite has a high dislocation density, which can greatly increase the hardness but reduce the low-temperature toughness. However, the grains after quenching present a very fine size, which can restrict the deterioration of these properties to some degree. Therefore, the decrease in the impact energy of the specimens obtained at 620 °C is limited. In addition, the specimens tempered at 620 °C produce a large number of acicular-tempered martensites, resulting in decreased impact toughness.

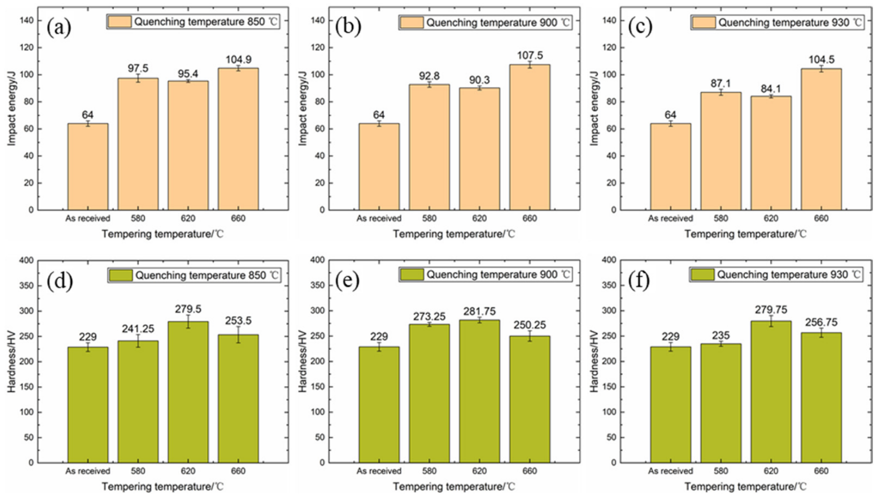

Figure 5. (**a**–**c**) Low-temperature (−40 °C) impact energy and (**d**,**e**) microhardness alterations with different quenching and tempering temperatures: (**a**,**d**) Q850 °C + T580, T620 and T660 °C, (**b**,**e**) Q900 °C + T580, T620 and T660 °C, and (**c**,**f**) Q930 °C + T580, T620 and T660 °C.

Figure 5d,e show the variation in hardness with different quenching and tempering processes. It can be clearly seen that the hardness values present an increasing trend followed by a decreasing trend when tempering from 580 to 660 °C. Specimens tempered at 620 °C always present relatively high hardness values due to the tempered martensite obtained with the largest volume fraction. However, the hardness values of the specimens tempered at 580 °C are not stable. The low hardness value of the specimen quenched at 850 °C and then tempered at 580 °C was due to the presence of a large number of polygonal ferrites, which cannot provide much strength. For the low hardness obtained in the specimen quenched at 930 °C and then tempered at 580 °C, the possible reasons are the relatively coarse grain size (Figure 4g) and the heterogeneity of each phase distribution.

Figure 6 shows the macroscopic fracture surfaces, which frequently consist of the fibrillar region, radial region, and shear slips. At the interface of the material, the fracture source first forms a fibrous fracture (Figure 6c); then, the crack expands rapidly, forming a radial fracture (Figure 6a), and finally forms a shear fracture (Figure 6b) on the three free surfaces of the notched specimen. When the specimen is subjected to the impact load, the tensile stress is obtained near the notched side, and the compressive stress is obtained on the other side of the fracture surface. When the fibrillar fracture of the tensile stress enters the compressive stress zone, the crack propagation is compressed and deformed, leading to the gradual disappearance of the fibrillar fracture. It is generally believed that the larger the fibrillar area and the shear lip area, the higher the toughness of the steel achieved. The bilateral arrows in Figure 6a–i mark the maximum width of the shear lip area, which is in good agreement with the impact energy results shown in Figure 5, indicating that the specimens tempered at a higher temperature of 660 °C (Figure 6c,f,i) with higher impact energies always obtain a wider shear lip than those attained in the specimens with lower tempering temperatures (Figure 6a,d,g for 580 °C and Figure 6b,e,h for 620 °C).

The fracture surfaces after impact tests for each heat treatment specimen were taken from the fibrillar regions, and are presented in Figure 7. It can be seen that almost all of the specimens present ductile fracture features. However, after comparing the specimens tempered at 580 °C (Figure 7a,d,g) and 660 °C (Figure 7c,f,i), the specimens tempered at 620 °C (Figure 7b,e,h) exhibit some heterogeneous fracture features with certain cleavage fracture surfaces, especially for the cases quenched at 900 and 930 °C. These show a good agreement with the impact results obtained in Figure 5a–c, indicating that the lowest impact toughness was also obtained at this tempering temperature. Large dimples together with ductile fracture bands and tear ridges are frequently produced due to the strong plastic deformation, and can be seen as the obstacles to crack propagation [16]. The fracture may be influenced by a variety of microstructural characteristics, such as a martensite packet consisting of several parallel plates inside [17]. It was proposed that M/A islands above 1 µm in size would be effortlessly split as the dislocation gliding was impeded, thus turning into crack initiation sites [18]. By comparison, it has been proposed that ferrite can offer a high amount of grain boundary areas, ascribed to the high volume of nucleation sites as well as high nucleation rates [15,19]. Meanwhile, soft ferrite can absorb a great amount of energy before fracture and ease the deformation stress concentration; hence, the cracking tendency can be diminished by comparison to the tempered martensite. Moreover, this can also disrupt and modify a crack propagation route at the interfaces of the harder and softer phase boundaries [20,21]. These may well prevent the propagation routes of cleavage cracks, reduce the stress concentration, and enhance the plastic deformation of the matrix accordingly, resulting in high toughness and crack-arrest capability of the material. In addition, it was suggested that the acicular ferrite staggered lath with a high-angle boundary can effectively improve the yield stress, toughness [17,22,23], and crack-arrest ability of the steel, subsequently obtaining superior impact resistance.

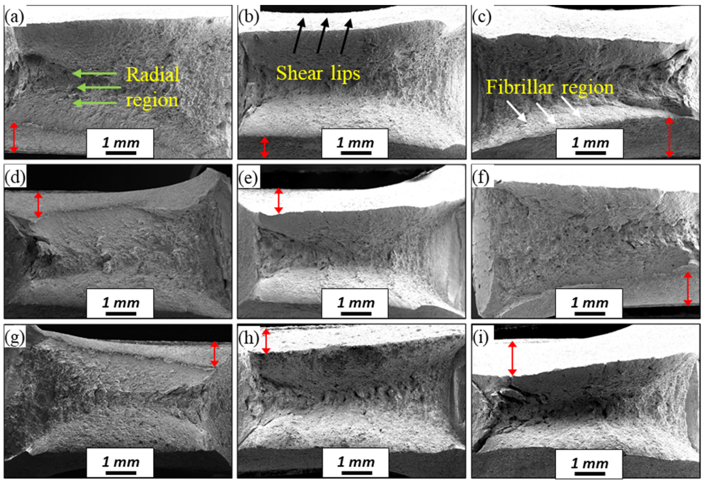

Figure 6. Macroscopic fractography of the low-temperature impact specimens with different quenching and tempering processes: (**a**) Q850 °C + T580 °C, (**b**) Q850 °C + T620 °C, (**c**) Q850 °C + T660 °C, (**d**) Q900 °C + T580 °C, (**e**) Q900 °C + T620 °C, (**f**) Q900 °C + T660 °C, (**g**) Q930 °C + T580 °C, (**h**) Q930 °C + T620 °C and (**i**) Q930 °C + T660 °C.

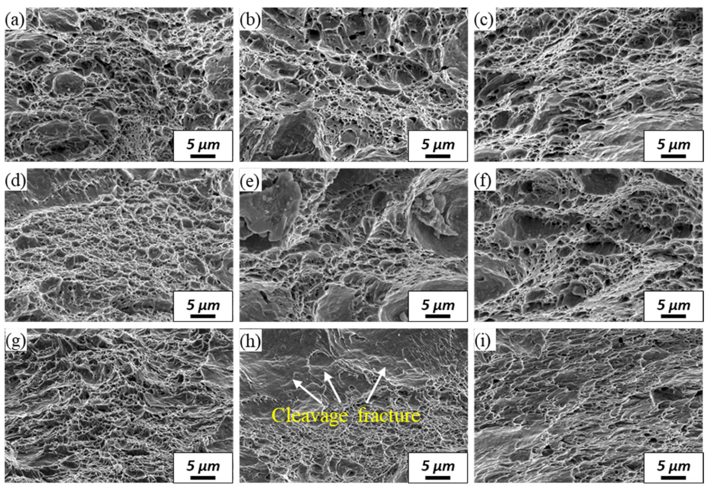

Figure 7. Fractography in the fibrillar region of the low-temperature impact specimens with different quenching and tempering processes: (**a**) Q850 °C + T580 °C, (**b**) Q850 °C + T620 °C, (**c**) Q850 °C + T660 °C, (**d**) Q900 °C + T580 °C, (**e**) Q900 °C + T620 °C, (**f**) Q900 °C + T660 °C, (**g**) Q930 °C + T580 °C, (**h**) Q930 °C + T620 °C and (**i**) Q930 °C + T660 °C.

3.3. Crystallographic Characterisation

To better understand the mechanisms in the results of impact energy variation (i.e., dropping at 620 °C but increasing at 660 °C tempering), the typical specimens (No. 2 and No. 6) mentioned hereinbefore were selected for EBSD analysis. The corresponding results of band contrast microstructure (Figure 8a–c) and inverse-pole figure maps (Figure 8d–f) are shown in Figure 8. In order to better compare the characterisation in different cases, the as-received material was also measured and analysed. It can be seen that as the quenching temperature increases, the amount of ferrite decreases steadily, and the island structure inside the tempered martensite grows sharply, which is favourable to enhance the strength of the material. Simultaneously, the existence of acicular ferrite ensures the high ductility of the material. It is supposed that the good notch-ductility of C-Mn steel is generally associated with a high proportion of acicular ferrite [24]. Consequently, the specimens quenched at relatively low temperatures (i.e., 850 and 900 °C) can have higher strength and toughness. When quenching at a higher temperature of 930 °C, the austenite grains grow coarser after full austenitisation. In this case, the primary microstructure contains the coarser tempered martensite grains generated after high-temperature quenching and tempering processes.

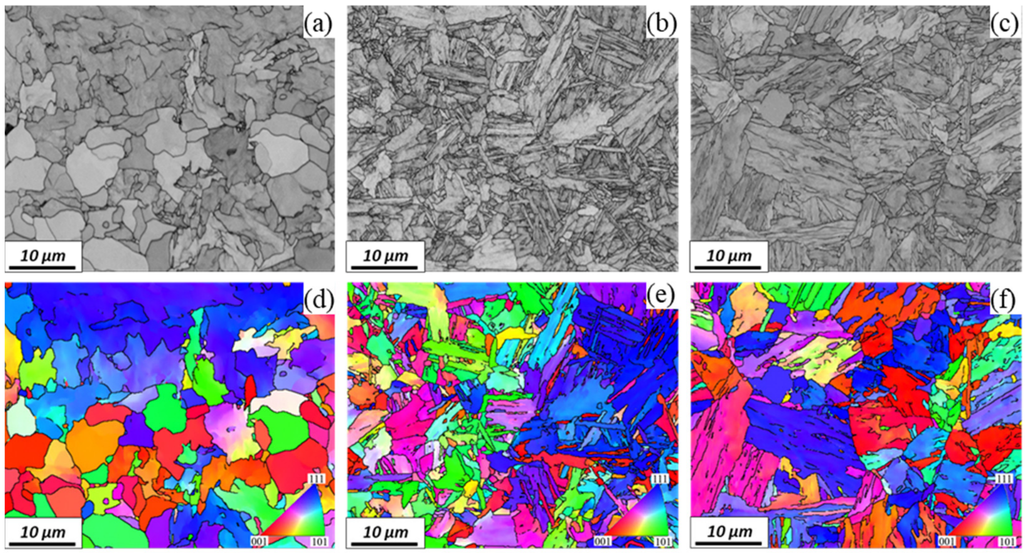

Figure 8. Band contrast and inverse-pole figure maps of (**a**,**d**) the as-received specimen, (**b**,**e**) specimen No. 2, and (**c**,**f**) specimen No. 6.

The polygonal ferrite structure, coarsening, and uneven grain size distribution are the three primary reasons leading to the reduced toughness. Lower toughness is achieved by the specimens with 620 °C tempering because the higher volume fraction of tempered martensite and a large number of granular grains result from the prior M/A islands. Even though the tempered martensite can provide much higher strength, it has a very limited ductility, leading to a decrease in the low-temperature ductility. Furthermore, M/A islands with granular features may have a variety of transition products or decomposition, which may cause a certain reduction in the low-temperature toughness [25].

In fact, effective grain size, the morphology of M/A islands, the distribution of second-phase particles, and the proportion of high/low-angle grain boundaries are the major factors influencing the low-temperature toughness. Figure 9 shows the high-angle grain boundaries (HAGBs, ≥15°) and low-angle grain boundaries (LAGBs, 3–15°) fraction comparison (Figure 9a–c), the grain boundary misorientation distribution (in Figure 9d–f), and the face-centred cubic (FCC) and body-centred cubic (BCC) distribution (in Figure 9g–i) of the as-received specimen, specimen No. 2, and specimen No. 6. It can be clearly seen that the specimen quenched at 900 °C and then tempered at 660 °C has fewer HAGBs (Figure 9a–c), but possesses more fractions of granular tempered martensite or retained austenite (Figure 9g–i). These granular features may relate to the occurrence of M/A islands with large, sharp angles. When deformation takes place, it leads to microcracks due to the stress concentration. However, it should be mentioned that the M/A islands and fine carbides continually precipitate adjacent to grain boundaries [26]. The small M/A islands can impede the dislocation growth and crack expansion due to stress concentration. In this case, these islands with a size of less than 1 µm can effectively increase the energy needed for crack propagation, and subsequently improve the toughness of the steel. Meanwhile, it has been reported that M/A islands of less than 0.5 µm in size can play a part in pinning dislocation movement, similar to the effects of precipitation-strengthening behaviour. In addition, low quenching temperatures lead to a high volume fraction of the coarse proeutectoid ferrite, which may diminish the strength and low-temperature toughness. High-temperature quenching and tempering treatments cause the austenite to be sliced by proeutectoid ferrite, which results in an increased volume fraction of the austenites, with uniform grain size and fine features.

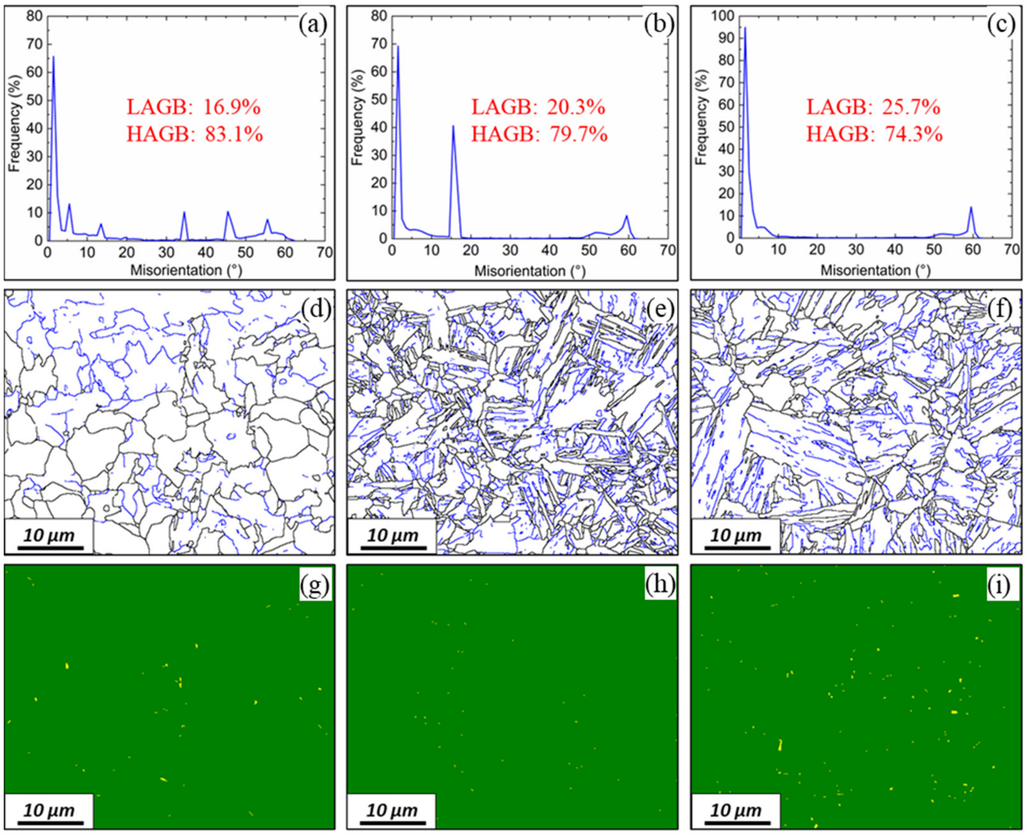

Figure 9. HAGB and LAGB fraction comparison, grain boundary misorientation distribution, and FCC and BCC distribution of (**a**,**d**,**g**) the as-received specimen, (**b**,**e**,**h**) specimen No. 2, and (**c**,**f**,**i**) specimen No. 6.

It has been widely reported that HAGBs improve the low-temperature toughness to varying degrees. However, the present study suggests that the quenched and tempered specimens with more LAGBs have higher low-temperature toughness. This may be largely because the retained austenite with the split martensite laths or blocks plays a more beneficial role in improving the low-temperature toughness than that with high-angle grain boundaries, which can decrease the effective grain size and prevent crack propagation.

Figure 10 presents the kernel average misorientation (KAM), GOS, and recrystallised fraction of the as-received specimen (Figure 10a,d,g), specimen No. 2 (Figure 10b,e,h), and specimen No. 6 (Figure 10c,f,i). The KAM results (Figure 10a–c) show the measurement of local grain misorientations for each selected specimen. It can be clearly seen that the specimens after heat treatments are more active than the as-received case. This is because there is large-scale phase transformation during the different quenching and tempering processes. In addition, the higher KAM always relates to more distributed local dislocation density, which is especially associated with the geometrically necessary dislocation [27]. In comparison, the GOS results for each selected specimen are shown in Figure 10d–f. Similar to the KAM results, the GOS results show that the specimens after quenching and tempering also have more variable grain orientations, suggesting a higher dislocation density distribution. Figure 10g–i illustrate the deformed (red), recrystallised (blue), and substructured (yellow) states, respectively. It should be mentioned that the deformed state here may mostly result from the interior stress obtained from the heat treatment. Clearly, specimen No. 2 shows the most complex combination of each state. This may be because there are extensive articular tempered martensites and ferrites in this heat treatment strategy. It can be clearly seen that specimen No. 6, after quenching and tempering, displays a more uniform distribution of each stated grain, suggesting better low-temperature toughness.

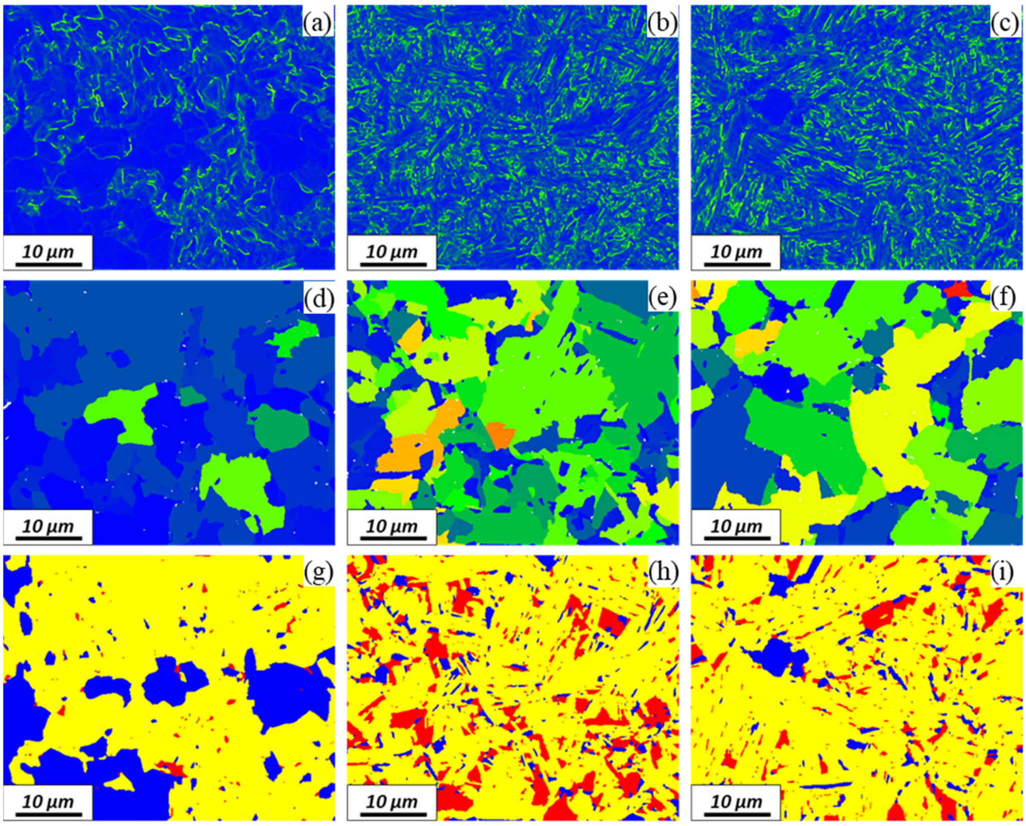

Figure 10. KAM, GOS, and deformed, recrystallised, and substructured fractions of (**a**,**d**,**g**) the as-received specimen, (**b**,**e**,**h**) specimen No. 2, and (**c**,**f**,**i**) specimen No. 6.

Figure 11 shows the characterised TEM results for specimen No. 2, with more complex microstructural features. It can be clearly seen that the tempered martensite laths (Figure 11c) are present, with an average lath spacing of 200–300 nm, in which high-density dislocations (Figure 11a,c) can exist. One possible explanation for these formations is that the quenching process results in a great number of weak mobility dislocations produced by phase transformation [15]. This quenched state possesses relatively high free energy, and can easily reach an equilibrium state with certain tempering processes. After this process, partial laths connect and coarsen to some extent, and then lead to the formation of subgrains during the tempering process. In this condition, more dislocations are activated, rearranged and, finally, generate dislocation walls. These dislocation walls are supposed to interconnect with one another and form the dislocation cell substructures, which can effectively hinder the crack propagation and improve the combination of strength and toughness. Meanwhile, the dislocation cell substructure suppresses the generation and propagation of microcracks due to the absorption of certain deformation energies. It should be mentioned that Figure 11b clearly shows the occurrence of feathery upper bainite. Bainite laths are supposed to be frequently generated from the prior austenite grain boundaries, which are slim and extended, and even penetrate the entire grain [15]. The amount of bainite lath always increases with higher quenching temperatures and drops with lower tempering temperatures. Once the crack propagates, the combined ferrite and bainite can hinder the further growth of the cracks by boosting energy consumption, enhancing the low-temperature toughness. In addition, a precipitate can be clearly seen in Figure 11d, and may contribute to the precipitate hardening to improve the yield strength.

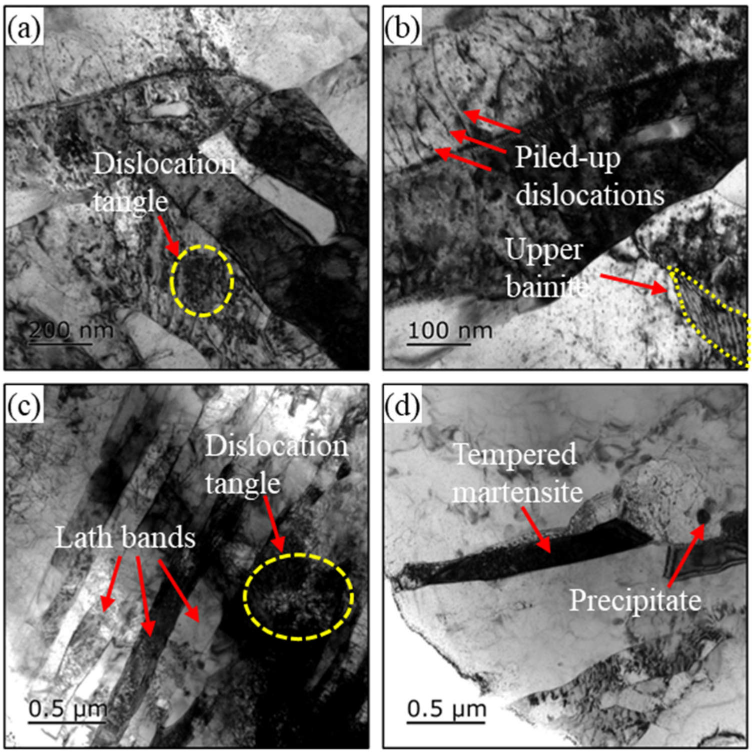

Figure 11. TEM images of different typical microstructural characterisations in specimen No. 2: (**a**) dislocation tangle, (**b**) piled-up dislocations and upper bainite, (**c**) lath bands and (**d**) tempered martensite and precipitate.

3.4. Effect of Microtexture on Toughness

The evolution of crystallographic microtexture can have an influence on the material's properties, including strength, anisotropy, ductility, and drawability [28,29]. Figure 12 shows the sections of φ_2 at 45°, 65°, and 90° from the complete ODFs of typical microtextural evolution. It can be clearly seen that specimens No. 2 (Figure 12b,e,h) and No. 6 (Figure 12c,f,i), after the corresponding quenching and tempering processes, show a great variance in the intensity of the typical rolling and fibre microtextures compared with that of the as-received specimen (Figure 12a,d,g). The microtexture in the as-received specimen is mainly located near the <110>//RD orientation. In fact, steels with a high volume fraction of <110>//RD orientation and a low volume fraction of <100>//RD have better low-temperature toughness [26]. In addition, it can be seen in Table 3, which gives the detailed volume fraction of each microtexture, that the as-received specimen has obtained the highest volume fraction of the cube ({001}<100>) orientation, which can facilitate crack propagation. Considering the lower impact properties obtained for the as-received specimen, it appears that the deterioration from the cube orientation plays a more important role in the low-temperature toughness compared to the improvement effects from the <100>//RD orientation.

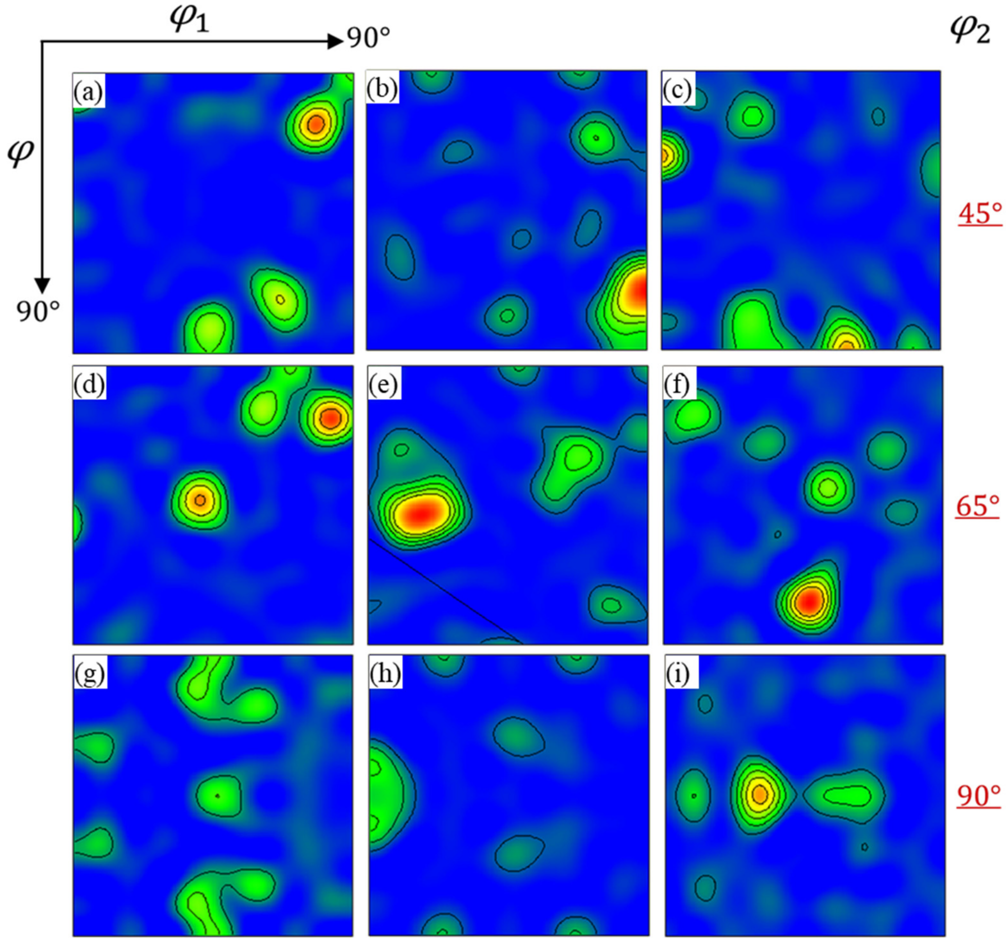

Figure 12. ODF maps of the as-received specimen (**a**,**d**,**g**), specimen No. 2 (**b**,**e**,**h**), and specimen No. 6 (**c**,**f**,**i**) at φ_2 = 45°, 65° and 90°.

Table 3. Volume fractions of the typical microtextures of the as-received specimen, specimen No. 2, and specimen No. 6.

Orientations	The As-Received Specimen	Specimen No. 2	Specimen No. 6
Cube	5.10%	0.68%	1.30%
Goss	0.50%	7.25%	2.19%
Brass	6.32%	1.15%	0.37%
Copper	0.0005%	13.00%	14.60%
S	3.93%	8.99%	11.00%
<111>//RD	2.55%	24.90%	17.30%
<110>//RD	49.50%	5.86%	24.70%
<100>//RD	11.60%	11.30%	4.00%

After different quenching and tempering processes, the microtexture is mainly concentrated near the {554}<225> orientation for specimen No. 2, and it has been suggested that this kind of orientation is beneficial to the drawing properties [30]. In comparison, the main microtexture of specimen No. 6 is rotated near the {110}<112> and {110}<111> orientations. In fact, the {100} crystal plane is regarded as the cleavage plane, which can lead to the occurrence of brittle cracks [31], while the {110} crystal plane is frequently regarded as the glide plane, which can benefit the dislocation slipping [32]. In addition, the {110} crystal plane can diminish the stress concentration generated from dislocation pile-up and, accordingly, impede the formation of microcracks [19]. Consequently, the crack sensitivity is lowered once the volume of the undesired {100} crystal plane is reduced and the amount of desired {110} crystal plane enlarges. Although both of these specimens obtained beneficial orientations for deformation, we would suggest that the preferred orientations derived in specimen No. 6 are more favourable than those derived from specimen No. 2, since higher low-temperature toughness was obtained.

4. Conclusions

This work investigated the effects of different quenching and tempering processes on the microstructural evolution, fracture mechanisms, and final properties—such as hardness and low-temperature toughness—of EH47 hull steel. The following conclusions can be drawn:

- Proper quenching and tempering heat treatment strategies can effectively ameliorate the combined properties in the form of high strength and low-temperature toughness.
- The specimens with 900 °C quenching and 660 °C tempering present a great phase mixture, giving the best combination of properties among all of the heat treatment strategies, owing to the comprehensive effect of the desired uniform distribution of each phase.
- The specimens tempered at 620 °C always obtain the highest hardness due to the higher contents of the tempered martensite.
- Relatively high quenching temperatures together with relatively low tempering temperatures help to significantly refine the grain size of the hull steel. In addition, certain retained austenites greatly contribute to the low-temperature impact properties.
- The specimens tempered at of 660 °C have higher impact energies due to the presence of longer shear lips than those in the specimens tempered at relatively low temperatures. By comparison, the specimens tempered at 620 °C exhibit some heterogeneous fracture features with certain cleavage fracture surfaces, especially for the cases quenched at 900 and 930 °C.
- Fewer high-angle grain boundaries but more fractions of granular tempered martensite or retained austenite can be detected in the specimen quenched at 900 °C and tempered at 660 °C.
- KAM and GOS results suggest that specimen No. 2 (850 °C quenching and 620 °C tempering) shows the most complex combination of each state, while specimen No. 6 (900 °C quenching and 660 °C tempering) displays a more uniform distribution of each stated grain. These properties are beneficial to the low-temperature toughness.
- Although specimens No. 2 (850 °C quenching and 620 °C tempering) and No. 6 (850 °C quenching and 620 °C tempering) both obtained beneficial orientations for deformation, the preferred orientations derived in specimen No. 6 are more favourable, owing to the higher obtained low-temperature toughness.

Author Contributions: Conceptualisation, H.Z., M.H. and Z.J.; methodology, H.Z.; software, M.H.; validation, M.H. and Z.M.; formal analysis, M.H., Z.M., H.W. and G.S.; investigation, L.L., T.Z., F.L. and F.C.; resources, H.Z. and Z.J.; data curation, M.H. and Z.M.; writing—original draft preparation, M.H.; writing—review and editing, H.Z. and Z.J.; visualisation, M.H.; supervision, Z.J.; project administration, Z.J.; funding acquisition, Z.J. All authors have read and agreed to the published version of the manuscript.

Funding: This research was funded by a grant from the State Key Laboratory of Metal Material for Marine Equipment and Applications, University of Science and Technology Liaoning co-projects, grant numbers SKLMEA-USTL 2017010 and 201905.

Institutional Review Board Statement: Not applicable.

Informed Consent Statement: Not applicable.

Data Availability Statement: Not applicable.

Conflicts of Interest: The authors declare no conflict of interest.

References

1. Youssef, S.; Noh, S.; Paik, J. A new method for assessing the safety of ships damaged by collisions. *Ships Offshore Struct.* **2017**, *12*, 862–872. [CrossRef]
2. Prabowo, A.R.; Baek, S.J.; Cho, H.J.; Byeon, J.H.; Bae, D.M.; Sohn, J.M. The Effectiveness of Thin-Walled Hull Structures against Collision Impact. *Lat. Am. J. Solids Struct.* **2017**, *14*, 1345–1360. [CrossRef]
3. Serreze, M.C.; Barry, R.G. *The Arctic Climate System*; Cambridge University Press: Cambridge, UK, 2014.
4. Zhang, H.; Yan, L.; Zhu, Y.; Ai, F.; Li, H.; Li, Y.; Jiang, Z. The Effect of Immersion Corrosion Time on Electrochemical Corrosion Behavior and the Corrosion Mechanism of EH47 Ship Steel in Seawater. *Metals* **2021**, *11*, 1317. [CrossRef]
5. Wu, H.; Li, Y.; Lu, Y.; Li, Z.; Cheng, X.; Hasan, M.; Zhang, H.; Jiang, Z. Influences of Load and Microstructure on Tribocorrosion Behaviour of High Strength Hull Steel in Saline Solution. *Tribol. Lett.* **2019**, *67*, 124. [CrossRef]
6. Li, L.; Xie, H.; Liu, T.; Li, X.; Liu, X.; Huo, M.; Wang, E.; Li, J.; Liu, H.; Sun, L.; et al. Effects of Rolling Force on Strip Shape during Tandem Cold Rolling Using a Novel Multistand Finite Element Model. *Steel Res. Int.* **2022**, *93*, 2100359. [CrossRef]
7. Zhang, H.M.; Li, Y.; Yan, L.; Ai, F.F.; Zhu, Y.Y.; Jiang, Z.Y. Effect of large load on the wear and corrosion behavior of high-strength EH47 hull steel in 3.5 wt% NaCl solution with sand. *Int. J. Miner. Metall. Mater.* **2020**, *27*, 1525–1535. [CrossRef]
8. Yu, D.; Chen, D.; Zheng, J.; He, Y.; Shen, F. Phase Transformation Unit of Bainitic Ferrite and its Surface Relief in Low and Medium Carbon Alloys Steels. *Acta Metall. Sin. (Engl. Lett.)* **2009**, *2*, 161–167.
9. Su, G.; Xie, H.; Huo, M.; Jia, F.; Wu, H.; Li, Z.; Bi, H.; Chang, E.; Xu, H.; Jiang, Z. Yielding Behavior and Strengthening Mechanisms of a High Strength Ultrafine-Grained Cr–Mn–Ni–N Stainless Steel. *Steel Res. Int.* **2022**, *93*, 2100524. [CrossRef]
10. Peet, M.J. 6-Bainitic steels and alloys for power plants. In *Structural Alloys for Power Plants*; Shirzadi, A., Jackson, S., Eds.; Woodhead Publishing: Sawston, UK, 2014; pp. 153–187.
11. Totten, G.E. *Steel Heat Treatment: Metallurgy and Technologies*; CRC Press: Boca Raton, FL, USA, 2006.
12. Krauss, G. *Steels: Processing, Structure, and Performance*; ASM International: Almere, The Netherlands, 2015.
13. Verhoeven, J.D. *Steel Metallurgy for the Non-Metallurgist*; ASM International: Almere, The Netherlands, 2007.
14. Smith, W.F.; Hashemi, J.; Presuel-Moreno, F. *Foundations of Materials Science and Engineering*; Mcgraw-Hill Publishing: New York, NY, USA, 2006.
15. Wan, D.C.; Cai, Q.W.; Yu, W.; Li, X.L.; Dong, C.Z. Effect of Heat Treatment Process on Microstructure and Properties of High Strength Heavy Plate for Ship Hull. *Adv. Mater. Res.* **2013**, *630*, 59–63. [CrossRef]
16. Huo, M.; Zhao, J.; Xie, H.; Li, S.; Zhang, H.; Hu, Z.; Jiang, Z. Microstructure and mechanical properties of thin varying thickness strips with different transition zones produced by micro flexible rolling. *Proc. Inst. Mech. Eng. Part B J. Eng. Manuf.* **2018**, *233*, 1954–1967. [CrossRef]
17. Brozzo, P.; Buzzichelli, G.; Mascanzoni, A.; Mirabile, M. Microstructure and cleavage resistance of low-carbon bainitic steels. *Met. Sci.* **1977**, *11*, 123–130. [CrossRef]
18. Chat, F.; Yang, C.-F.; Zhang, Y.-Q.; Xu, Z. Effect of granular bainite on impact toughness of CGHAZ of ultra-low carbon copper-bearing age-hardening steel. *J. Iron Steel Res.* **2005**, *17*, 42–46. (In Chinese)
19. Wu, J.Y.; Wang, B.; Wang, B.X.; Misra, R.D.K.; Wang, Z.D. Toughness and ductility improvement of heavy EH47 plate with grain refinement through inter-pass cooling. *Mater. Sci. Eng. A* **2018**, *733*, 117–127. [CrossRef]
20. Kim, Y.M.; Kim, S.K.; Lim, Y.J.; Kim, N.J. Effect of Microstructure on the Yield Ratio and Low Temperature Toughness of Linepipe Steels. *ISIJ Int.* **2002**, *42*, 1571–1577. [CrossRef]
21. Hwang, B.; Lee, C.G.; Kim, S.-J. Low-Temperature Toughening Mechanism in Thermomechanically Processed High-Strength Low-Alloy Steels. *Metall. Mater. Trans. A* **2011**, *42*, 717–728. [CrossRef]
22. Díaz, M.; Madariaga, I.; Rodriguez-Ibabe, J.M.; Gutierrez, I. Improvement of mechanical properties in structural steels by development of acicular ferrite microstructures. *J. Constr. Steel Res.* **1998**, *46*, 413–414. [CrossRef]
23. Chen, J.; Tang, S.; Liu, Z.-Y.; Wang, G.-D. Microstructural characteristics with various cooling paths and the mechanism of embrittlement and toughening in low-carbon high performance bridge steel. *Mater. Sci. Eng. A* **2013**, *559*, 241–249. [CrossRef]
24. Zhang, C.; Gong, B.; Deng, C.; Wang, D. Computational prediction of mechanical properties of a C-Mn weld metal based on the microstructures and micromechanical properties. *Mater. Sci. Eng. A* **2017**, *685*, 310–316. [CrossRef]
25. Wu, J.; Wang, B.; Wang, B.; Misra, R.D.K.; Wang, Z. Influence of Inter-Pass Cooling on Microstructural Evolution and Plastic Deformation of Heavy EH47 Plates. *Materials* **2019**, *12*, 1686. [CrossRef]
26. Tian, Y.; Wang, H.T.; Ye, Q.B.; Wang, Q.H.; Wang, Z.D.; Wang, G.D. Effect of rolling reduction below γ non-recrystallization temperature on pancaked γ, microstructure, texture and low-temperature toughness for hot rolled steel. *Mater. Sci. Eng. A* **2020**, *794*, 139640. [CrossRef]
27. Calcagnotto, M.; Ponge, D.; Demir, E.; Raabe, D. Orientation gradients and geometrically necessary dislocations in ultrafine grained dual-phase steels studied by 2D and 3D EBSD. *Mater. Sci. Eng. A* **2010**, *527*, 2738–2746. [CrossRef]
28. Kaijalainen, A.J.; Suikkanen, P.; Karjalainen, L.P.; Jonas, J.J. Effect of Austenite pancaking on the microstructure, texture, and bendability of an ultrahigh-strength strip steel. *Metall. Mater. Trans. A Phys. Metall. Mater. Sci.* **2014**, *45*, 1273–1283. [CrossRef]
29. Huo, M.; Zhao, J.; Xie, H.; Jia, F.; Li, S.; Zhang, H.; Jiang, Z. Effects of micro flexible rolling and annealing on microstructure, microhardness and texture of aluminium alloy. *Mater. Charact.* **2019**, *148*, 142–155. [CrossRef]

30. Salinas, A.; Artigas, A.; Perez-Ipiña, J.; Castro-Cerda, F.; Garza-Montes-de-Oca, N.; Colás, R.; Petrov, R.; Monsalve, A. Effects of Heat Treatment on Morphology, Texture, and Mechanical Properties of a MnSiAl Multiphase Steel with TRIP Behavior. *Metals* **2018**, *8*, 1021. [CrossRef]
31. Wang, C.; Wu, X.; Liu, J.; Xu, N.a. Transmission electron microscopy of martensite/austenite islands in pipeline steel X70. *Mater. Sci. Eng. A* **2006**, *438–440*, 267–271. [CrossRef]
32. Nafisi, S.; Arafin, M.A.; Collins, L.; Szpunar, J. Texture and mechanical properties of API X100 steel manufactured under various thermomechanical cycles. *Mater. Sci. Eng. A* **2012**, *531*, 2–11. [CrossRef]